HHS Public Access

Author manuscript

J Comp Neurol. Author manuscript; available in PMC 2022 January 01.

Published in final edited form as:

J Comp Neurol. 2021 January ; 529(1): 221–233. doi:10.1002/cne.24944.

LRRTM4 is a member of the transsynaptic complex between rod photoreceptors and bipolar cells

Melina A. Agosto[1,*], **Theodore G. Wensel**[1]

[1]Verna and Marrs McLean Department of Biochemistry and Molecular Biology, Baylor College of Medicine, Houston, Texas, United States

Abstract

Leucine rich repeat transmembrane (LRRTM) proteins are synaptic adhesion molecules with roles in synapse formation and signaling. LRRTM4 transcripts were previously shown to be enriched in rod bipolar cells (BCs), secondary neurons of the retina that form synapses with rod photoreceptors. Using two different antibodies, LRRTM4 was found to reside primarily at rod BC dendritic tips, where it colocalized with the transduction channel protein, TRPM1. LRRTM4 was not detected at dendritic tips of ON-cone BCs. Following somatic knockout of LRRTM4 in BCs by subretinal injection and electroporation of CRISPR/Cas9, LRRTM4 was abolished or reduced in the dendritic tips of transfected cells. Knockout cells had a normal complement of TRPM1 at their dendritic tips, while GPR179 accumulation was partially reduced. In experiments with heterologously expressed protein, the extracellular domain of LRRTM4 was found to engage in heparan-sulfate dependent binding with pikachurin. These results implicate LRRTM4 in the GPR179-pikachurin-dystroglycan transsynaptic complex at rod synapses.

Graphical abstract

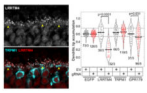

Leucine rich repeat transmembrane (LRRTM) proteins are synaptic adhesion molecules with roles in synapse formation and signaling. LRRTM4 was found to reside at rod bipolar cell (BC) dendritic tips, where it colocalized with the transduction channel protein, TRPM1. LRRTM4 was not detected at dendritic tips of ON-cone BCs. Following somatic knockout of LRRTM4 in BCs by subretinal injection and electroporation of CRISPR/Cas9, LRRTM4 was abolished or reduced in the dendritic tips of transfected cells. Knockout cells had a normal complement of TRPM1 at their dendritic tips, while GPR179 accumulation was partially reduced. In experiments with heterologously expressed protein, the extracellular domain of LRRTM4 was found to engage in

[*]Correspondence: Melina A. Agosto, Department of Biochemistry and Molecular Biology, BCM-125, Baylor College of Medicine, 1 Baylor Plaza, Houston, TX 77030, agosto@bcm.edu.

Data availability statement: The data that support the findings of this study are available from the corresponding author upon reasonable request.

Conflict of interest: The authors declare no conflicts of interest.

Ethics approval statement: All animal procedures were approved by the Baylor College of Medicine Animal Care and Use Committee.

heparansulfate dependent binding with pikachurin. These results implicate LRRTM4 in the GPR179-pikachurin-dystroglycan transsynaptic complex at rod synapses.

Keywords

rod bipolar cell; rod photoreceptor; synaptic adhesion molecule; LRRTM4; pikachurin; RRID: CVCL_0045; RRID: IMSR_CRL: 22; RRID:Addgene_59313; RRID:Addgene_18817; RRID:Addgene_18817; RRID:AB_2138196; RRID:AB_2284227; RRID:AB_2336642

1. Introduction

Transsynaptic interactions are critical for the development and maintenance of synapses, and play important roles in encoding specificity in wiring of neural circuits (Siddiqui & Craig, 2011; Sudhof, 2018; Williams et al., 2010). In the mammalian retina, rod and cone photoreceptors deliver inputs to the ON pathway by synaptic transmission to rod bipolar cells (BCs) and ON-cone BCs, respectively (Dunn & Wong, 2014). These two types of synapses set up functionally distinct circuits: the primary rod pathway, which responds to dim light, and the cone pathway, which functions in photopic conditions. The mechanisms underlying specific synapse formation between the correct cell types are mostly unknown.

Rod and ON-cone BCs have many post-synaptic proteins in common, including the G_o-coupled metabotropic glutamate receptor mGluR6 (Masu et al., 1995; Nawy, 1999; Vardi, 1998) and GTPase accelerating protein (GAP) complexes consisting of $G_{\beta 5S}$ bound either to RGS7 and the orphan GPCR GPR179 or to RGS11 and R9AP (Audo et al., 2012; Cao et al., 2009, 2012; Peachey et al., 2012; Rao et al., 2007; Ray et al., 2014; Sarria et al., 2016; Shim et al., 2012). Several transsynaptic interactions have been identified at photoreceptor-BC synapses. Presynaptic ELFN1, a leucine-rich repeat (LRR) protein, interacts transsynaptically with mGluR6; ELFN1 is selectively expressed in rods, and specifically contributes to rod-rod BC synapse formation (Cao et al., 2015). However, the post-synaptic target, mGluR6, is present on both rod and cone ON-BCs. LRIT3, another LRR protein expressed presynaptically, can interact with postsynaptic nyctalopin (Hasan et al., 2019, 2020). Although LRIT3 and nyctalopin are present at both rod and cone synapses, and knockout of LRIT3 disrupts postsynaptic localization of nyctalopin and TRPM1 at both, other post-synaptic proteins are selectively affected at cone BCs (Hasan et al., 2019, 2020; Neuillé et al, 2015). Finally, pikachurin, a heparan sulfate proteoglycan (HSPG) expressed by photoreceptors and secreted into the synaptic cleft, interacts with presynaptic dystroglycan and post-synaptic GPR179 (Orlandi et al., 2018; Sato et al., 2008). GPR179 and pikachurin are located at both rod and cone synapses (Ray et al., 2014; Sato et al., 2008). To date, no postsynaptic candidates for specific transsynaptic interactions at the rod synapses have been identified.

The leucine rich repeat transmembrane neuronal (LRRTM) proteins are a family of cell adhesion proteins found in vertebrates, consisting of four members (LRRTM1–4) (Roppongi et al., 2017). Like ELFN1, LRIT3, and nyctalopin, LRRTM proteins have an LRR-containing extracellular N-terminal domain, a single transmembrane helix, and a Cterminal cytoplasmic domain. LRRs encode a conserved structural motif shaped like a curved

solenoid (Barton et al., 2003; Bella et al., 2008; Paatero et al., 2016; Yamagata et al., 2018). The variable positions in the LRR consensus sequence allow for different protein interaction interfaces, and LRR proteins have been implicated in many functions. All four LRRTM proteins are expressed postsynaptically, have synaptogenic activity, and induce presynaptic differentiation at excitatory synapses (Linhoff et al., 2009). LRRTM13 bind in trans with presynaptic neurexins (Ko et al., 2009; Siddiqui et al., 2010; Um et al., 2016; de Wit et al., 2009). LRRTM4 mediates its synaptogenic activity by binding presynaptic glypicans or neurexins, both in a heparan-sulfate (HS) dependent manner (Roppongi et al., 2020; Siddiqui et al., 2013), and is important for excitatory synapse development in dentate gyrus granule cells and cortical neurons (Siddiqui et al., 2013; de Wit et al., 2013).

In the retina, LRRTM4 transcripts are enriched specifically in rod BCs (Shekhar et al., 2016; Woods et al., 2018), and expression in BCs was confirmed by in situ hybridization (Shekhar et al., 2016) and immunofluorescence (Woods et al., 2018), although subcellular localization was not determined. A mutation in the LRRTM4 cytoplasmic domain was associated with macular degeneration in a human family, in which electroretinogram findings resembled a no-b-wave (nob) phenotype (Kawamura et al., 2018), suggesting impairment of signal transmission at the photoreceptor-BC synapse (McCall & Gregg., 2008; Zeitz et al., 2015). Recently, rod BC terminals were found to have altered morphology and function in LRRTM4 knockout mice (Sinha et al., 2020). Here, we show that LRRTM4 is specifically localized at the dendritic tips of rod BCs, and has the ability to interact transsynaptically with pikachurin. Somatic knockout of LRRTM4 using CRISPR/Cas9 suggests a role in organizing the GAP complex containing GPR179.

2. Materials and Methods

2.1. Cells.

Human embryonic kidney (HEK293) cells (ATCC #CRL-1573, RRID: CVCL_0045) and Cos-7 cells (ATCC) were maintained in DMEM (Corning) supplemented with 10% FBS (Sigma), in a 37°C humidified incubator with 5% CO_2 atmosphere.

2.2. Animals.

All procedures were approved by the Baylor College of Medicine Animal Care and Use Committee. WT C57BL/6 mice were purchased from the Baylor College of Medicine Center for Comparative Medicine, and used for all experiments except electroporations. WT CD-1 mice were used for all electroporations, and were obtained from Charles River Laboratories (RRID: IMSR_CRL: 22). Absence of $Pde6b^{rd1}$ and $Crb1^{rd8}$ retina degeneration alleles was confirmed by PCR and sequencing (Gimenez & Montoliu, 2001; Mattapallil et al., 2012).

2.3. DNA constructs.

Mouse pikachurin (Egflam) cDNA (BC095994) was obtained from Transomic, and the open reading frame was cloned with a C-terminal 1D4 tag into pCDNA3.1. Mouse LRRTM4 cDNA (BC037216) was from Origene, and mouse ELFN1 cDNA was from Dharmacon (Clone Id: 6811341). The extracellular domain of LRRTM4 (residues 1–425) and the extracellular domain of ELFN1 (residues 1–418) were cloned as fusions with human Fc,

derived from Addgene plasmid #59313 (a gift from Peter Scheiffele and Tito Serafini; RRID:Addgene_59313), in pcDNA3.1, to make LRRTM4(NT)-Fc and ELFN1(NT)-Fc. pGrm6P-EGFP, containing the Grm6 promoter 200 bp critical region along with SV40 enhancer (Kim et al, 2008), was constructed from Addgene plasmid #18817 (a gift from Connie Cepko; RRID:Addgene_18817) by removing the IRES and alkaline phosphatase portions of the sequence. mGluR6 cDNA (NP_775548.2) was cloned from mouse retina cDNA as described (Kang et al, 2014) and pGrm6P-mGluR6-EGFP was made by replacing EGFP in pGrm6P-EFP with a mGluR6GGGSGGG-EGFP fusion connected with a 7-aa flexible linker.

To perform CRISPR/Cas9 gene editing specifically in ON BCs, the Grm6 promoter 200 bp critical region along with SV40 enhancer (Kim et al., 2008) from pGrm6P was cloned into pX458 (Ran et al., 2013) (a gift from Feng Zhang; RRID:Addgene_48138) XbaI/AgeI sites, replacing the Cbh promoter and intron and resulting in pX458-Grm6P. Target sequences for CRISPR knockout were chosen with guidance from the Broad Institute GPP sgRNA Designer tool (Doench et al., 2016) and cloned into BbsI sites in pX458-Grm6P by ligating annealed oligos. Oligos were (target sequences underlined): gRNA-1, 5’ CACCGGCTGCTGGTTATGCTGACGG-3’ and 5’-AAACCCGTCAGCATAACCAGCAGCC-3’; gRNA-2, 5’-CACCGTCCCTGAGAACATTTCTGGA-3’ and 5’-AAACTCCAGAAATGTTCTCAGGGAC-3’.

2.4. Pull-down assays.

HEK293 or Cos-7 cells were transfected with polyethylenimine Max (PEI) (molecular weight 40,000; Polysciences). Cells in 10-cm dishes with 15 ml of serum-free DMEM were transfected with 12 μg of plasmid DNA mixed with 60 μl of 1 mg/ml PEI in 1.5 ml of serum-free DMEM supplemented with 20 mM HEPES, pH 7.4; transfections were scaled down 5-fold for cells in 6-well plates. Medium was replaced with serum-containing medium after 2–3 h. For purification of LRRTM4(NT)-Fc, IgGdepleted serum (Sigma) was used. 3–4 days post-transfections, cell culture supernatants (TC sups) were harvested, centrifuged to remove cells, and supplemented with 50 mM Tris pH 7.4 or pH 8, 0.02% sodium azide, and a dash of solid phenylmethylsulfonyl fluoride.

Preparation of 1D4 antibody from hybridoma culture and conjugation to CNBractivated Sepharose 4B (GE Healthcare) were previously described (Agosto et al., 2014). 1D4Ab-conjugated beads were mixed with pikachurin-1D4 TC sup and incubated with gentle agitation at 4°C overnight. Mock beads were prepared either with serumcontaining media, or with TC sup from mock-transfected cells; no differences were observed with these reagents. Beads were washed with PBS supplemented with Complete Protease Inhibitor mix (Roche), and eluted with 1D4 peptide (TETSQVAPA) (Genscript) 5 mg/ml in wash buffer, pH ~7. For experiments with bead-bound pikachurin, beads were used directly after washing, without eluting. LRRTM4(NT)-Fc was purified from TC sup (with low-IgG serum) using a protein G Sepharose 4 Fast Flow (GE Healthcare) column equilibrated in PBS. The column was washed in PBS, and eluted with 0.1 M Glycine, pH 2.7. Eluates were neutralized with 100 mM Tris pH 8.

Pull-down experiments with purified proteins were performed in pika buffer (PBS with 1.5 mM KCl, 2 mM $CaCl_2$, 2 mM $MgCl_2$, and 0.5% Triton X-100). Reactions containing both proteins, or control reactions containing pikachurin only, were incubated on ice for 1 h, mixed with Protein G agarose beads (Pierce) and incubated for 1 h on a roller at 4°C, and washed with pika buffer. For pull-down experiments from TC sup, pikachurin-bound beads or control beads were mixed with TC sup containing 0.5% Triton X-100, incubated for 90 min on a roller at 4°C, and washed with pika buffer. Heparinase treatments were performed with heparinase III from *Flavobacterium heparinum* (Sigma #H8891) reconstituted in 20 mM Tris, 4 mM $CaCl_2$, pH 7.4. One volume of bead-bound pikachurin in PBS with Complete protease inhibitors was diluted with ~2 volumes of Hep buffer (20 mM Tris, 100 mM NaCl, 40 mM $CaCl_2$, pH 7.4) and treated with 1 U/ml heparinase, or mock buffer, for 1 h at 37°C. Beads were washed with PBS and used for pull-down experiments as described above. Samples were assessed by SDS-PAGE and western blotting with 1D4 antibody conjugated to IRDye-680LT NHS ester (Licor) according to the manufacturer instructions (~0.2 ug/ml) and IRDye-800CW anti-human IgG (Licor, 1:5000), and imaged on an Odyssey infrared scanner (Licor).

2.5. Subretinal injection and electroporation.

WT CD-1 albino neonates (P0) were used for all injections. DNA was prepared using Qiagen maxiprep or Qiafilter maxiprep kits (Qiagen) and dissolved in water. For injections, DNA was mixed with 10X PBS and 0.1% Fast Green dye such that the final concentrations were 1X PBS, 0.1% dye, and ~3.8 mg/ml total DNA (1.2 mg/ml pGrm6P-mGluR6-EGFP and either 1.3 mg/ml each of pX458-Grm6P-LRRTM4gRNA-1 and pX458-Grm6P-LRRTM4gRNA-2, or 2.6 mg/ml pX458-Grm6P empty vector). Injections and electroporations were performed as described (Matsuda & Cepko, 2004, 2008). Eyelids were opened at the future edge of the eyelid, a pilot hole was made in the sclera with a 30G needle, and a 33G blunt injection needle was inserted in the pilot hole and positioned in the subretinal space at the far side of the eye. ~450 nl of injection mix was delivered by microinjector (UMP3 Microsyringe Injector and Micro4 Controller, World Precision Instruments) set at 130 nl/s. Five 50-ms pulses of 80 V, separated by 950 ms, were applied across the eyes using custom tweezers with 7mm diameter electrodes and an ECM 830 square wave electroporator (BTX Harvard Apparatus).

2.6. Immunofluorescence labeling and microscopy.

C57BL/6 mice were processed at 1–3 months of age. Injected CD-1 animals were processed at 4–6 weeks of age. Whole eyes were fixed in 2% PFA in PBS for 10 min at RT, or as indicated in the figure legends. A range of fixation times and PFA concentrations were tested, and 2% PFA for 10 min was the least harsh condition that provided good preservation of morphology. Following fixation, eyes were washed extensively with PBS, and cryoprotected in 30% sucrose in PBS overnight at 4°C. Corneas were removed, eyecups with lenses were embedded in OCT, and 10–12 μm sections were cut. Sections were blocked for 2 h at RT in PBS with 10% donkey serum, 5% BSA, and 0.2% Triton X-100, incubated overnight at 4°C with primary antibodies diluted in blocking buffer, washed in PBS, then incubated at RT for ~2 h with Alexa fluor-conjugated secondary antibodies (Invitrogen/Thermo Fisher) diluted to 8 μg/ml in blocking buffer. For simultaneous detection of IgG1

and IgG2b mouse antibodies, isotype-specific secondary antibodies were used. Finally, slides were washed in PBS and mounted with Prolong Diamond (Invitrogen/Thermo Fisher) and #1.5 thickness coverglass.

Images were acquired with a Zeiss LSM-710 confocal microscope using a 63X oil immersion objective (Zeiss, Plan-Apochromat 63x/1.4 Oil DIC M27) with Immersol 518F immersion oil (Zeiss). Alexa 647, Alexa 555, and EGFP were detected sequentially with 633 nm HeNe laser, 561 nm DPSS laser, and 488 nm Argon laser. Some images were acquired with a Leica TCS-SP5 confocal microscope using a 63X oil immersion objective (Leica, HC PL APO CS2 63.0X, numerical aperture 1.40) with Type F immersion oil (Leica); Alexa 555 and Alexa 488 were detected sequentially with 543 nm HeNe and 488 nm Argon laser lines. Emission regions were set to avoid cross-talk between the channels, and images were acquired with few or no saturated pixels. Single optical sections (~0.7–1.4 μm thickness) were acquired unless indicated otherwise. In some cases, alignment of channels was corrected manually. Corrections were performed with full images (not individual puncta), using large features such as cell bodies, visible in all channels as background and/or cross-talk fluorescence using extreme brightness settings, as a guide.

2.7. Primary antibodies.

Primary antibodies used for immunofluorescence were: LRRTM4 clone N205B/22 (Millipore #MABN828) (10 μg/ml), used for all figures except Figure 1c; validation: this study. LRRTM4 alternate antibody (R&D systems #AF5377; RRID:AB_2138196) (1:40), used in Figure 1c (LRRTM4 B). GPR179 sheep polyclonal antibody (1:1000) was a gift from Ronald Gregg, University of Louisville; this antibody was validated by immunofluorescence in $Gpr179^{nob5/nob5}$ mouse retina tissue (Peachey et al., 2012). TRPM1 clone 545H5 (8–10 μg/ml) was generated and purified as described (Agosto et al., 2014), and validated with Trpm1 KO mouse retina (Agosto et al., 2018). PKCα (Cell Signaling #2056; RRID:AB_2284227) (1:200). Rhodamine-labeled peanut agglutinin (PNA) (Vector Labs #RL-1072; RRID:AB_2336642) (~1:110). A previously validated pikachurin antibody (Sato et al., 2008) was not available, and a different antibody (GeneTex #GTX 117855) did not label photoreceptor synapses in mouse retina.

2.8. Image analysis and quantification.

For display, images were processed in ImageJ (NIH) and/or Photoshop (Adobe) to apply pseudocolors and adjust the minimum and maximum input levels. For quantitative analyses, raw images from the Zeiss microscope (33 nm/px) were used (with channel alignment if necessary, as described in Section 2.6). Puncta meeting the following criteria were chosen: (1) orientation such that two tips were clearly visible, (2) signal in all antibody channels, (3) GFP signal present in one (and only one) of the tips, and (4) not touching or overlapping other bright staining in any channel. Each 1024-px image yielded 1–7 puncta meeting these criteria. The same set of puncta were used for both line profile and dendritic tip accumulation analyses.

Line profiles were obtained in ImageJ using 4 px wide lines and the “plot profile” tool, and analyzed in Mathematica 12 (Wolfram). Profiles were first normalized to minimum and

maximum values, and the first and last values greater than half of the maximum (left and right edges) were determined. The width at half max was calculated from the difference of the two edges, and the width of EGFP overlap was calculated as the intersection of the two [left edge, right edge] intervals.

Dendritic tip accumulation was analyzed using 50 pixel square regions cropped from Zeiss images (33 nm/px). Raw images were used (with channel alignment if necessary, as described in Section 2.6), except in cases where neighboring features were present within the 50 px image that were brighter than the puncta of interest and thus interfering with downstream processing, channels were manually edited to replace the conflicting feature with a middle grey value. Images were processed in Mathematica. Raw images from each channel were first scaled to [0,1], then thresholded at 0.5, i.e. all pixel values ≤0.5 were set to 0. A mask was created by binarizing the thresholded EGFP channel (setting all non-zero pixels to 1), then applying the *MorphologicalComponents* function with method "ConvexHull", keeping only the largest component and omitting any touching the borders, and binarizing again. The mask was applied to the other thresholded channels using *ImageMultiply*, and the total intensity of the remaining pixels were measured. This measurement was then normalized by dividing by the total number of pixels in the mask.

3. Results

3.1. LRRTM4 is specifically localized to rod BC dendritic tips

Immunostaining with a LRRTM4 monoclonal antibody revealed punctate labeling in the OPL (Figure 1a). This staining pattern was sensitive to fixation, with harsher fixation resulting in severely diminished detection of OPL puncta (Figure 1a, right). The LRRTM4 puncta co-localized with TRPM1 in rod BC dendritic tips; however, little or no LRRTM4 was detected in cone ON-BC dendritic tips, marked by the lectin PNA (yellow arrowheads, Figure 1b). Identical results were obtained with a polyclonal antibody raised against a different, non-overlapping, fragment of LRRTM4 (Figure 1c). Results with CRISPR knockout of LRRTM4, described below, further validate the specificity of LRRTM4 immunostaining. Detection of LRRTM4 in rod BC dendritic tips, but not cone BC tips, is consistent with the observed enrichment of LRRTM4 transcripts specifically in rod BCs (Shekhar et al., 2016; Woods et al., 2018).

LRRTM4 was previously reported to be located at rod BC axon terminals (Sinha et al., 2020). In imaging and processing conditions suitable for detection of OPL puncta, staining in the inner plexiform layer (IPL) was unremarkable (Figures 1a, 2). However, slightly brighter immunolabeling was observed on rod BC axons/terminals, marked by PKCα (Figure 2b).

3.2. The LRRTM4 extracellular domain interacts with pikachurin

Since LRRTM4 was previously shown to bind HSPGs (Siddiqui et al., 2013), we hypothesized that it may also interact with pikachurin, a HSPG expressed by photoreceptors and secreted into the synaptic cleft (Sato et al., 2008). Pikachurin-1D4 purified from HEK293 or Cos7 cell culture supernatant was heparan sulfated, as evidenced by the slow

migration of the protein in SDS-PAGE gels, and the appearance of a faster-migrating band upon heparinase treatment (Figure 3a,d). Purified Pikachurin coprecipitated with purified LRRTM4 extracellular domain fused to Fc (LRRTM4(NT)-Fc) (Figure 3b), and in reciprocal experiments, bead-bound pikachurin co-precipitated LRRTM4(NT)-Fc from cell culture supernatant (Figure 3c). ELFN1 extracellular domain, in contrast, was not precipitated (Figure 3c). The interaction between pikachurin and LRRTM4 was HS-dependent, as treatment with heparinase greatly reduced binding (Figure 3d). This mode of binding is consistent with the HS-dependent LRRTM4 binding to glypicans (Siddiqui et al., 2013), but distinct from GPR179-pikachurin binding, which is maintained following heparinase treatment (Orlandi et al., 2018).

3.3. Somatic CRISPR knockout of LRRTM4

To knockout LRRTM4 in postnatal mice, plasmid DNA expressing a CRISPR gRNA, along with Cas9 expressed under control of the Grm6 promoter (Kim et al., 2008), was introduced by subretinal injection and electroporation at P0 (Matsuda & Cepko, 2004). A similar strategy was used previously for somatic knockout of ON-BC genes (Sarin et al., 2018), using coexpressed EGFP to identify transfected cells. However, although the Cas9 cassette also expresses EGFP following a T2A self-cleaving peptide (see Methods), we found EGFP expression in ON-BCs to be weak, and difficult to identify in dendritic tips. Therefore, a Grm6 promoter plasmid expressing mGluR6-EGFP was co-injected with the CRISPR plasmid. Previous work has shown that injection of multiple plasmids results in nearly complete coincidence of expression in the same cells (Tang et al., 2013). mGluR6-EGFP was correctly localized to ON BC dendritic tips (Figure 4); it colocalized with TRPM1 OPL puncta, but was often detected in only one of the two BC tips present in a synapse (Figure 4b–d), consistent with synaptic participation of dendrites from one transfected cell and one untransfected cell. This is unsurprising, since electroporation results in sparse transfection, and the two BC dendritic tips in a synapse almost always belong to two different BCs (Behrens et al., 2016).

At low magnification, differences in LRRTM4 immunostaining were typically subtle, consistent with sparse knockout and transfected cells paired at synapses with untransfected cells (Figure 5). However, closer examination of puncta revealed that in dendritic tip pairs in which EGFP was detected in one tip, LRRTM4 expression was detected predominantly in the opposing tip (Figure 6a). In control animals injected with Cas9 vector lacking a gRNA (empty vector), LRRTM4 staining was similar in both tips (Figure 6a). Analysis of line profiles (Figure 6c) through dendritic tip pairs showed that the width of LRRTM4 labeling was significantly reduced in the EGFP-containing puncta, while TRPM1 was unaffected (Figure 6d). Overlap of LRRTM4 with EGFP was significantly reduced, indicating that LRRTM4 expression is specifically affected in the EGFP-containing tip (Figure 6e). These results demonstrate successful somatic knockout of a post-synaptic protein in ON-BCs, and further validate the immunolocalization of LRRTM4 at the rod BC dendritic tips.

3.4. GPR179 dendritic tip accumulation is slightly reduced in LRRTM4 knockout BCs

Since the LRRTM4 extracellular domain interacted in vitro with pikachurin, we hypothesized that LRRTM4 ablation may affect pikachurin accumulation or function at the

synapse. Since we were unable to obtain a satisfactory pikachurin antibody, we sought to indirectly test this hypothesis by measuring accumulation of GPR179, a postsynaptic protein that is mislocalized in pikachurin knockout animals (Orlandi et al., 2018). With the line profile method of quantifying puncta widths and EGFP overlap, GPR179 immunostaining appeared to be unaffected by LRRTM4 knockout (Figure 6d–e). However, manual inspection of the profiles revealed that the relative intensity of GPR179 labeling was partially reduced in some of the EGFP-containing tips (Figure 6b). Therefore, we employed a more rigorous image analysis method to quantify dendritic tip accumulation in the EGFP-containing tips (Figure 7). With this quantification method, LRRTM4 dendritic tip accumulation was severely reduced, while TRPM1 was unaffected, as found with the other analysis methods. However, GPR179 accumulation was slightly, but significantly (p = 0.031), reduced, suggesting a role for LRRTM4 in stabilizing the GPR179-pikachurin complex (Figure 7d).

4. Discussion

Our results show that the synaptic adhesion protein LRRTM4 is located specifically at rod BC dendritic tips (Figure 1). The dendritic tip localization was observed with two different antibodies, and was abolished or greatly reduced in dendritic tips transfected with LRRTM4-targeted CRISPR/Cas9 (Figures 6–7), validating this finding. However, it was recently reported that LRRTM4 was localized to rod BC terminals, although other layers of the retina were not shown (Sinha et al., 2020). Though the antibody used in that study was previously shown to specifically detect LRRTM4 in the dentate gyrus, validated using a LRRTM4 KO mouse (Siddiqui et al., 2013), validation of specific immunostaining in the rod BC terminals was not shown (Sinha et al., 2020). We also observed faint (relative to background) labeling of rod BC terminals (Figure 2), although the specificity of this labeling pattern was not determined. Discrepancies in immunolocalization could be due to differences in fixation conditions, which we found to have a strong effect on the detection of dendritic tip labeling (Figure 1a), or to differences among antibodies. LRRTM4 may be located at both dendritic tips and axon terminals of rod BCs. Some other cell adhesion molecules have been localized to different sides of synapses in different cell types; for example, the LRR-containing protein ELFN1 is presynaptic at the rod-rod BC synapse (Cao et al., 2015), but postsynaptic at excitatory synapses in other neurons (Sylwestrak & Ghosh, 2012; Tomioka et al., 2014). The LRRTM4 KO mouse was found to have significant structural and functional abnormalities at rod BC terminals, implicating LRRTM4 in a functional role at the terminals (Sinha et al., 2020). Another possibility is that alterations in rod-rod BC synapse formation or function during development could result in abnormalities in the BC axon terminals in the LRRTM4 KO. In a previous study, TRPM1 KO mice were found to have rod BCs with abnormal terminal morphology and fewer connections with amacrine cells, phenotypes which were attributed to a requirement for TRPM1 channel opening during development (Kozuka et al., 2017).

The involvement of LRRTM4 in transsynaptic interactions and synaptogenesis in other neurons (Roppongi et al., 2020; Siddiqui et al., 2013; de Wit et al., 2013) potentially implicates LRRTM4 in formation of rod-rod BC synapses. Indeed, we observed a direct HS-dependent interaction between the LRRTM4 extracellular domain and pikachurin, a synaptic

cleft HSPG present at photoreceptor-BC synapses (Figure 3). This result is consistent with the reported interactions of LRRTM4 with presynaptic glypicans and neurexins, which are both HS dependent (Roppongi et al., 2020; Siddiqui et al., 2013). We also observed, at some puncta, a reduction in GPR179 dendritic tip accumulation in LRRTM4 CRISPR knockout BCs (Figure 7), suggesting a role in organizing or stabilizing the GPR179-pikachurin transsynaptic interaction (Orlandi et al., 2018). Unlike pikachurin and GPR179, which are present at both rod and cone synapses (Ray et al., 2014; Sato et al., 2008), LRRTM4 was found to be specifically expressed in rod BCs (Figure 1). This expression pattern suggests the presence of different transsynaptic complexes involving the GAP complex at rod and cone synapses, which may have roles in specific wiring of the rod and cone pathways during development.

The small and heterogeneous reduction in GPR179 signal at dendritic tips in LRRTM4 KO cells (Figures 6 and 7) may indicate a role in development that is not critical at postnatal stages, or the presence of a protein with a redundant function. Consistent with the latter possibility, LRRTM4 KO mice were reported to have no deficit in light-evoked depolarization of rod BCs (Sinha et al., 2020). On the other hand, while GPR179 KO mice have a nob ERG phenotype (Peachey et al., 2012; Ray et al., 2014), pikachurin KO mice, in which GPR179 dendritic tip localization is reduced by more than half, have scotopic b-waves with delayed implicit time and only partially reduced amplitudes (Orlandi et al., 2018; Sato et al., 2008). Thus a reduction in pikachurin or GPR179 accumulation in the absence of LRRTM4 may not result in a severe defect in BC light responses. It is also possible that there are ultrastructural defects not observed with the limited resolution of confocal microscopy, as was the the case in the pikachurin KO mouse – a defect in BC dendrite insertion into the synapse was evident by electron microscopy, but not by conventional light microscopy (Sato et al., 2008). In addition to the limited spatial resolution, the conclusions are also limited by potential artifacts resulting from the image analysis methods. For instance, EGFP overlap measurements (but not width measurements) are sensitive to misalignment of the different imaging channels. Furthermore, puncta from each image were chosen for analysis based on visual assessment of orientation and labeling (described in Section 2.8). If any puncta with severe abnormalities were present, such that two tips were not visible, or labeling with any antibody was missing in both tips, they were not included.

A missense mutation in the cytoplasmic C-terminus of LRRTM4 was associated with autosomal dominant macular degeneration and nob ERGs (Kawamura et al., 2018), which are characteristic of complete congenital stationary night blindness patients. This disorder is associated with mutations in genes encoding proteins required for synaptic transmission between photoreceptors and ON BCs, including nyctalopin, mGluR6, TRPM1, GPR179, and LRIT3 (Zeitz et al., 2015), and the nob phenotype is recapitulated in knockout or otherwise non-expressing mouse models (Gregg et al., 2007; Masu et al., 1995; Morgans et al., 2009; Neuillé et al., 2014; Peachey et al., 2012; Shen et al., 2009). However, as rod BC depolarization was reported to be normal in LRRTM4 KO retina (Sinha et al., 2020), in this case the nob phenotype observed with the LRRTM4 mutation may reflect a dominant negative function imparted by the mutant cytoplasmic domain, and so is not necessarily contradictory with observations from the LRRTM4 KO mouse. The link between LRRTM4

and macular degeneration is unclear. While we and others (Shekhar et al., 2016; Woods et al., 2018) have shown selective expression of LRRTM4 in rods, the macula, unlike the rest of the human retina, is cone-dense. However, rods remain more abundant than cones in most of the macula (Bringmann et al., 2018), and one possibility is that cone degeneration is secondary to rod degeneration (Narayan et al., 2016), although the reason for specific involvement of the macula is unknown. Other possibilities are that there is a low level of expression in cone BCs that is poorly detected in our immunofluorescence staining conditions, that LRRTM4 is differentially expressed in different cell types during development, or that LRRTM4 has different roles in mice and humans. Further studies are needed to understand the role of LRRTM4 in retina development and photoreceptor health.

Acknowledgements:

This work was supported by Welch Foundation grant Q0035, and NIH grants R01-EY026545 and R01-EY025218 to T.G.W.

References

Agosto MA, Anastassov IA, & Wensel TG (2018). Differential epitope masking reveals synapse-specific complexes of TRPM1. Visual Neuroscience, 35, e001. [PubMed: 29370879]

Agosto MA, Zhang Z, He F, Anastassov IA, Wright SJ, McGehee J, & Wensel TG (2014). Oligomeric state of purified transient receptor potential melastatin-1 (TRPM1), a protein essential for dim light vision. Journal of Biological Chemistry, 289, 27019–27033.

Audo I, Bujakowska K, Orhan E, Poloschek CM, Defoort-Dhellemmes S, Drumare I, Kohl S, Luu TD, Lecompte O, Zrenner E, Lancelot M-E, Antonio A, Germain A, Michiels C, Audier C, Letexier M, Saraiva J-P, Leroy BP, Munier FL, … Zeitz C (2012). Whole-exome sequencing identifies mutations in GPR179 leading to autosomal-recessive complete congenital stationary night blindness. American Journal of Human Genetics, 90, 321–330. [PubMed: 22325361]

Barton WA, Liu BP, Tzvetkova D, Jeffrey PD, Fournier AE, Sah D, Cate R, Strittmatter SM, & Nikolov DB (2003). Structure and axon outgrowth inhibitor binding of the Nogo-66 receptor and related proteins. EMBO Journal, 22, 3291–3302.

Behrens C, Schubert T, Haverkamp S, Euler T, & Berens P (2016). Connectivity map of bipolar cells and photoreceptors in the mouse retina. eLife, 5, e20041.

Bella J, Hindle KL, McEwan PA, & Lovell SC (2008). The leucine-rich repeat structure. Cellular and Molecular Life Sciences, 65, 2307–2333. [PubMed: 18408889]

Bringmann A, Syrbe S, Görner K, Kacza J, Francke M, Wiedemann P, & Reichenbach A (2018). The primate fovea: Structure, function and development. Progress in Retinal and Eye Research, 66, 49–84. [PubMed: 29609042]

Cao Y, Masuho I, Okawa H, Xie K, Asami J, Kammermeier PJ, Maddox DM, Furukawa T, Inoue T, Sampath AP, & Martemyanov KA (2009). Retinaspecific GTPase accelerator RGS11/Gβ5S/R9AP is a constitutive heterotrimer selectively targeted to mGluR6 in ON-bipolar neurons. Journal of Neuroscience, 29, 9301–9313. [PubMed: 19625520]

Cao Y, Pahlberg J, Sarria I, Kamasawa N, Sampath AP, & Martemyanov KA (2012). Regulators of G protein signaling RGS7 and RGS11 determine the onset of the light response in ON bipolar neurons. Proceedings of the National Academy of Sciences of the United States of America, 109, 7905–7910. [PubMed: 22547806]

Cao Y, Sarria I, Fehlhaber KE, Kamasawa N, Orlandi C, James KN, Hazen JL, Gardner MR, Farzan M, Lee A, Baker S, Baldwin K, Sampath AP, & Martemyanov KA (2015). Mechanism for selective synaptic wiring of rod photoreceptors into the retinal circuitry and its role in vision. Neuron, 87, 1248–1260. [PubMed: 26402607]

Doench JG, Fusi N, Sullender M, Hegde M, Vaimberg EW, Donovan KF, Smith I, Tothova Z, Wilen C, Orchard R, Virgin HW, Listgarten J, & Root DE (2016). Optimized sgRNA design to maximize activity and minimize offtarget effects of CRISPR-Cas9. Nature Biotechnology, 34, 184–191.

Dunn FA, & Wong ROL (2014). Wiring patterns in the mouse retina: collecting evidence across the connectome, physiology and light microscopy. Journal of Physiology, 592, 4809–4823.

Gimenez E, & Montoliu L (2001). A simple polymerase chain reaction assay for genotyping the retinal degeneration mutation (Pdeb rd1) in FVB/N-derived transgenic mice. Laboratory Animals, 35, 153–156. [PubMed: 11315164]

Gregg RG, Kamermans M, Klooster J, Lukasiewicz PD, Peachey NS, Vessey KA, & McCall MA (2007). Nyctalopin expression in retinal bipolar cells restores visual function in a mouse model of complete X-linked congenital stationary night blindness. Journal of Neurophysiology, 98, 3023–3033. [PubMed: 17881478]

Hasan N, Pangeni G, Cobb CA, Ray TA, Nettesheim ER, Ertel KJ, Lipinski DM, McCall MA, & Gregg RG (2019). Presynaptic expression of LRIT3 transsynaptically organizes the postsynaptic glutamate signaling complex containing TRPM1. Cell Reports, 27, 3107–3116. [PubMed: 31189098]

Hasan N, Pangeni G, Ray TA, Fransen KM, Noel J, Borghuis BG, McCall MA, & Gregg RG (2020). LRIT3 is required for Nyctalopin expression and normal ON and OFF pathway signaling in the retina. eNeuro, 7, ENEURO.0002–20.2020

Kang HJ, Menlove K, Ma J, Wilkins A, Lichtarge O, & Wensel TG (2014). Selectivity and evolutionary divergence of metabotropic glutamate receptors for endogenous ligands and G proteins coupled to phospholipase C or TRP channels. Journal of Biological Chemistry, 289, 29961–29974.

Kawamura Y, Suga A, Fujimaki T, Yoshitake K, Tsunoda K, Murakami A, & Iwata T (2018). LRRTM4-C538Y novel gene mutation is associated with hereditary macular degeneration with novel dysfunction of ON-type bipolar cells. Journal of Human Genetics, 63, 893–900. [PubMed: 29760528]

Kim DS, Matsuda T, & Cepko CL (2008). A core paired-type and POU homeodomain-containing transcription factor program drives retinal bipolar cell gene expression. Journal of Neuroscience, 28, 7748–7764. [PubMed: 18667607]

Ko J, Fuccillo MV, Malenka RC, & Sudhof TC (2009). LRRTM2 functions as a neurexin ligand in promoting excitatory synapse formation. Neuron, 64, 791–798. [PubMed: 20064387]

Kozuka T, Chaya T, Tamalu F, Shimada M, Fujimaki-Aoba K, Kuwahara R, Watanabe SI, & Furukawa T (2017). The TRPM1 channel is required for development of the rod ON bipolar cell-AII amacrine cell pathway in the retinal circuit. Journal of Neuroscience, 37, 9889–9900. [PubMed: 28899920]

Linhoff MW, Lauren J, Cassidy RM, Dobie FA, Takahashi H, Nygaard HB, Airaksinen MS, Strittmatter SM, & Craig AM (2009). An unbiased expression screen for synaptogenic proteins identifies the LRRTM protein family as synaptic organizers. Neuron, 61, 734–749. [PubMed: 19285470]

Masu M, Iwakabe H, Tagawa Y, Miyoshi T, Yamashita M, Fukuda Y, Sasaki H, Hiroi K, Nakamura Y, Shigemoto R, Takada M, Nakamura K, Nakao K, Katsuki M, & Nakanishi S (1995). Specific deficit of the ON response in visual transmission by targeted disruption of the mGluR6 gene. Cell, 80, 757–765. [PubMed: 7889569]

Matsuda T, & Cepko CL (2004). Electroporation and RNA interference in the rodent retina in vivo and in vitro. Proceedings of the National Academy of Sciences of the United States of America, 101, 16–22. [PubMed: 14603031]

Matsuda T, & Cepko CL (2008). Analysis of gene function in the retina. Methods in Molecular Biololgoy, 423, 259–278.

Mattapallil MJ, Wawrousek EF, Chan C-C, Zhao H, Roychoudhury J, Ferguson TA, & Caspi RR (2012). The rd8 mutation of the Crb1 gene is present in vendor lines of C57BL/6N mice and embryonic stem cells, and confounds ocular induced mutant phenotypes. Investigative Ophthalmology & Visual Science, 53, 2921–2927. [PubMed: 22447858]

McCall MA, & Gregg RG (2008). Comparisons of structural and functional abnormalities in mouse b-wave mutants. Journal of Physiology, 586, 4385–4292.

Morgans CW, Zhang J, Jeffrey BG, Nelson SM, Burke NS, Duvoisin RM, & Brown RL (2009). TRPM1 is required for the depolarizing light response in retinal ON-bipolar cells. Proceedings of the National Academy of Sciences of the United States of America, 106, 19174–19178. [PubMed: 19861548]

Narayan DS, Wood JP, Chidlow G, & Casson RJ (2016). A review of the mechanisms of cone degeneration in retinitis pigmentosa. Acta ophthalmologica, 94, 748–754. [PubMed: 27350263]

Nawy S (1999). The metabotropic receptor mGluR6 may signal through G(o), but not phosphodiesterase, in retinal bipolar cells. Journal of Neuroscience, 19, 2938–2944. [PubMed: 10191311]

Neuillé M, El Shamieh S, Orhan E, Michiels C, Antonio A, Lancelot ME, Condroyer C, & Bujakowska K (2014). Lrit3 deficient mouse (nob6): a novel model of complete congenital stationary night blindness (cCSNB). PLoS One, 9, e90342

Neuillé M, Morgans CW, Cao Y, Orhan E, Michiels C, Sahel J-A, Audo I, Duvoisin RM, Martemyanov KA, & Zeitz C (2015). LRIT3 is essential to localize TRPM1 to the dendritic tips of depolarizing bipolar cells and may play a role in cone synapse formation. European Journal of Neuroscience, 42, 1966–1975.

Orlandi C, Omori Y, Wang Y, Cao Y, Ueno A, Roux MJ, Condomitti G, de Wit J, Kanagawa M, Furukawa T, & Martemyanov KA (2018). Transsynaptic binding of orphan receptor GPR179 to dystroglycan-pikachurin complex is essential for the synaptic organization of photoreceptors. Cell Reports, 25, 130–145. [PubMed: 30282023]

Paatero A, Rosti K, Shkumatov AV, Sele C, Brunello C, Kysenius K, Singha P, Jokinen V, Huttunen H, & Kajander T (2016). Crystal structure of an engineered LRRTM2 synaptic adhesion molecule and a model for neurexin binding. Biochemistry, 55, 914–926. [PubMed: 26785044]

Peachey NS, Ray TA, Florijn R, Rowe LB, Sjoerdsma T, Contreras-Alcantara S, Baba K, Tosini G, Pozdeyev N, Iuvone PM, Bojang P, Pearring JN, Simonsz HJ, van Genderen M, Birch DG, Traboulsi EI, Dorfman A, Lopez I, Ren H, … & Gregg, R. G. (2012). GPR179 is required for depolarizing bipolar cell function and is mutated in autosomal-recessive complete congenital stationary night blindness. American Journal of Human Genetics, 90, 331–339. [PubMed: 22325362]

Ran FA, Hsu PD, Wright J, Agarwala V, Scott DA, & Zhang F (2013). Genome engineering using the CRISPR-Cas9 system. Nature Protocols, 8, 2281–2308. [PubMed: 24157548]

Rao A, Dallman R, Henderson S, & Chen C-K (2007). Gβ5 is required for normal light responses and morphology of retinal ON-bipolar cells. Journal of Neuroscience, 27, 14199–14204. [PubMed: 18094259]

Ray TA, Heath KM, Hasan N, Noel JM, Samuels IS, Martemyanov KA, Peachey NS, McCall MA, & Gregg RG (2014). GPR179 is required for high sensitivity of the mGluR6 signaling cascade in depolarizing bipolar cells. Journal of Neuroscience, 34, 6334–6343. [PubMed: 24790204]

Roppongi RT, Dhume SH, Padmanabhan N, Silwal P, Zahra N, Karimi B, Bomkamp C, Patil CS, Champagne-Jorgensen K, Twilley RE, Zhang P, Jackson MF, & Siddiqui TJ (2020). LRRTMs organize synapses through differential engagement of neurexin and PTPσ. Neuron, 10.1016/j.neuron.2020.01.003.

Roppongi RT, Karimi B, & Siddiqui TJ (2017). Role of LRRTMs in synapse development and plasticity. Neuroscience Research, 116, 18–28. [PubMed: 27810425]

Sarin S, Zuniga-Sanchez E, Kurmangaliyev YZ, Cousins H, Patel M, Hernandez J, Zhang KX, Samuel MA, Morey M, Sanes JR, & Zipursky SL (2018). Role for Wnt signaling in retinal neuropil development: Analysis via RNA-Seq and in vivo somatic CRISPR mutagenesis. Neuron, 98, 109–126. [PubMed: 29576390]

Sarria I, Orlandi C, McCall MA, Gregg RG, & Martemyanov KA (2016). Intermolecular interaction between anchoring subunits specify subcellular targeting and function of RGS proteins in retina ON-bipolar neurons. Journal of Neuroscience, 36, 2915–25. [PubMed: 26961947]

Sato S, Omori Y, Katoh K, Kondo M, Kanagawa M, Miyata K, Funabiki K, Koyasu T, Kajimura N, Miyoshi T, Sawai H, Kobayashi K, Tani A, Toda T, Usukura J, Tano Y, Fujikado T, & Furukawa T

(2008). Pikachurin, a dystroglycan ligand, is essential for photoreceptor ribbon synapse formation. Nature Neuroscience, 11, 923–931. [PubMed: 18641643]

Shekhar K, Lapan SW, Whitney IE, Tran NM, Macosko EZ, Kowalczyk M, Adiconis X, Levin JZ, Nemesh J, Goldman M, McCarroll SA, Cepko CL, Regev A, & Sanes JR (2016). Comprehensive classification of retinal bipolar neurons by single-cell transcriptomics. Cell, 166, 1308–1323. [PubMed: 27565351]

Shen Y, Heimel JA, Kamermans M, Peachey NS, Gregg RG, & Nawy S (2009). A transient receptor potential-like channel mediates synaptic transmission in rod bipolar cells. Journal of Neuroscience, 29, 6088–6093. [PubMed: 19439586]

Shim H, Wang C-T, Chen Y-L, Chau VQ, Fu KG, Yang J, McQuiston AR, Fisher RA, & Chen C-K (2012). Defective retinal depolarizing bipolar cells in regulators of G protein signaling (RGS) 7 and 11 double null mice. Journal of Biological Chemistry, 287, 14873–14879.

Siddiqui TJ, & Craig AM (2011). Synaptic organizing complexes. Current Opinion in Neurobiology, 21, 132–143. [PubMed: 20832286]

Siddiqui TJ, Pancaroglu R, Kang Y, Rooyakkers A, & Craig AM (2010). LRRTMs and neuroligins bind neurexins with a differential code to cooperate in glutamate synapse development. Journal of Neuroscience, 30, 7495–7506. [PubMed: 20519524]

Siddiqui TJ, Tari PK, Connor SA, Zhang P, Dobie FA, She K, Kawabe H, Wang YT, Brose N, & Craig AM (2013). An LRRTM4-HSPG complex mediates excitatory synapse development on dentate gyrus granule cells. Neuron, 79, 680–95. [PubMed: 23911104]

Sinha R, Siddiqui TJ, Padmanabhan N, Wallin J, Zhang C, Karimi B, Rieke F, Craig AM, Wong RO, & Hoon M (2020). LRRTM4: A novel regulator of presynaptic inhibition and ribbon synapse arrangements of retinal bipolar cells. Neuron, 105, 1007–1017. [PubMed: 31974009]

Sudhof TC (2018). Towards an understanding of synapse formation. Neuron, 100, 276–293. [PubMed: 30359597]

Sylwestrak EL, & Ghosh A (2012). Elfn1 regulates target-specific release probability at CA1-interneuron synapses. Science, 338, 536–540. [PubMed: 23042292]

Tang JCY, Szikra T, Kozorovitskiy Y, Teixiera M, Sabatini BL, Roska B, & Cepko CL (2013). A nanobody-based system using fluorescent proteins as scaffolds for cell-specific gene manipulation. Cell, 154, 928–939. [PubMed: 23953120]

Tomioka NH, Yasuda H, Miyamoto H, Hatayama M, Morimura N, Matsumoto Y, Suzuki T, Odagawa M, Odaka YS, Iwayama Y, Won Um J, Ko J, Inoue Y, Kaneko S, Hirose S, Yamada K, Yoshikawa T, Yamakawa K, & Aruga J (2014). Elfn1 recruits presynaptic mGluR7 in trans and its loss results in seizures. Nature Communications, 5, 4501.

Um JW, Choi T-Y, Kang H, Cho YS, Choii G, Uvarov P, Park D, Jeong D, Jeon S, Lee D, Kim H, Lee S-H, Bae Y-C, Choi S-Y, Airaksinen MS, & Ko J (2016). LRRTM3 regulates excitatory synapse development through alternative splicing and neurexin binding. Cell Reports, 14, 808–822. [PubMed: 26776509]

Vardi N (1998). Alpha subunit of G(o) localizes in the dendritic tips of ON bipolar cells. Journal of Comparative Neurology, 395, 43–52.

Williams ME, de Wit J, & Ghosh A (2010). Molecular mechanisms of synaptic specificity in developing neural circuits. Neuron, 68, 9–18. [PubMed: 20920787]

de Wit J, O'Sullivan ML, Savas JN, Condomitti G, Caccese MC, Vennekens KM, Yates JR 3rd, & Ghosh A (2013). Unbiased discovery of glypican as a receptor for LRRTM4 in regulating excitatory synapse development. Neuron, 79, 696–711. [PubMed: 23911103]

de Wit J, Sylwestrak E, O'Sullivan ML, Otto S, Tiglio K, Savas JN, Yates JR 3rd, Comoletti D, Taylor P, & Ghosh A (2009). LRRTM2 interacts with neurexin1 and regulates excitatory synapse formation. Neuron, 64, 799–806. [PubMed: 20064388]

Woods SM, Mountjoy E, Muir D, Ross SE, & Atan D (2018). A comparative analysis of rod bipolar cell transcriptomes identifies novel genes implicated in night vision. Scientific Reports, 8, 5506. [PubMed: 29615777]

Yamagata A, Goto-Ito S, Sato Y, Shiroshima T, Maeda A, Watanabe M, Saitoh T, Maenaka K, Terada T, Yoshida T, Uemura T, & Fukai S (2018). Structural insights into modulation and selectivity of transsynaptic neurexin-LRRTM interaction. Nature Communications, 9, 3964.

Zeitz C, Robson AG, & Audo I (2015). Congenital stationary night blindness: an analysis and update of genotype-phenotype correlations and pathogenic mechanisms. Progress in Retinal and Eye Research, 45, 58–110. [PubMed: 25307992]

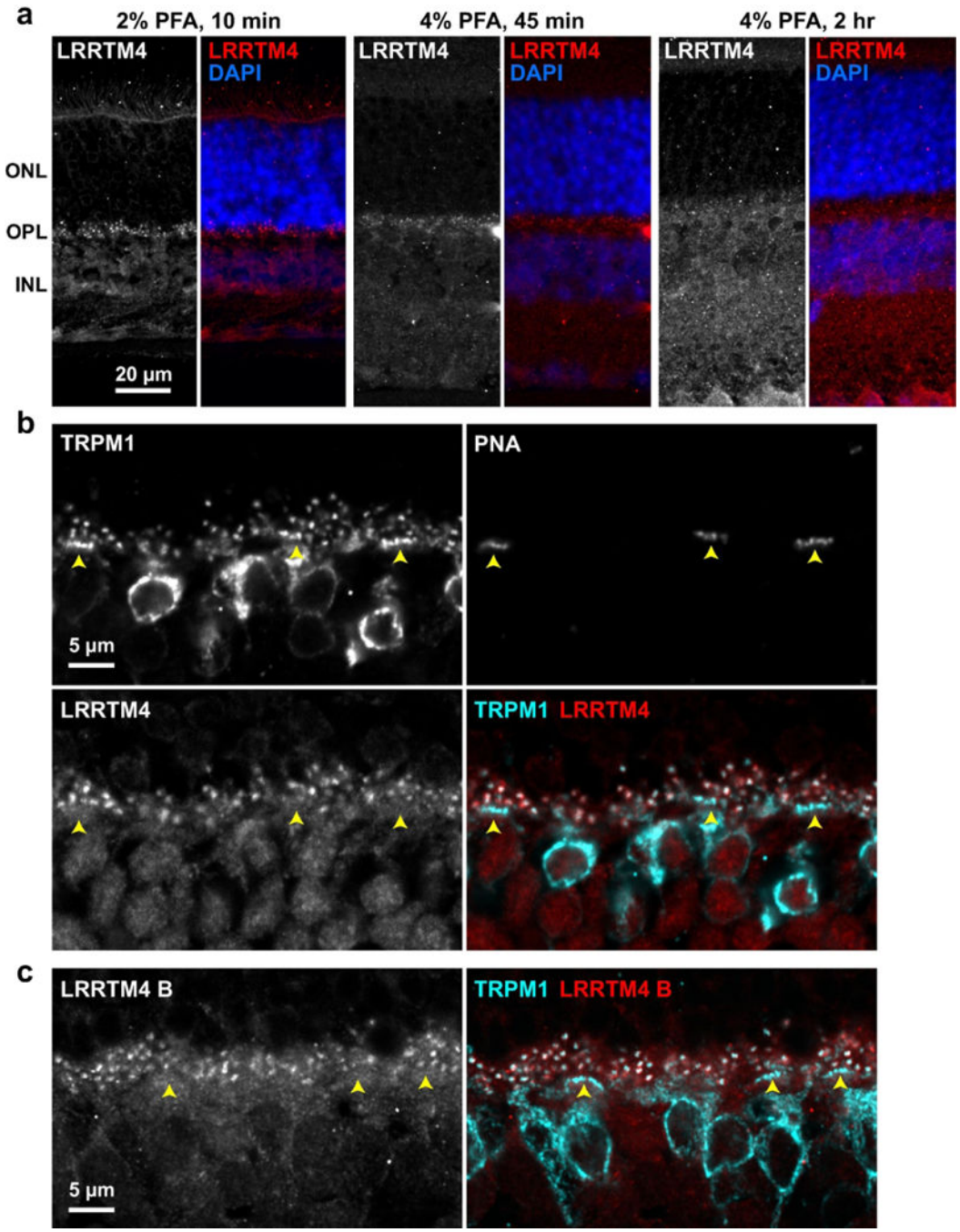

Figure 1. LRRTM4 is localized at rod BC dendritic tips.

(**a**) Comparison of fixation conditions. After fixation with 2% PFA for 10 min (left) LRRTM4 immunoreactivity is predominantly located in OPL puncta. Harsher fixation (middle, right) resulted in large reductions in overall fluorescence intensity and loss of dendritic tip labeling. Images are shown with varying adjustments to input levels such that the background fluorescence is visible across conditions. The lightest fixation condition (2% PFA for 10 min) was used in all subsequent experiments. (**b**) LRRTM4 puncta colocalize with rod dendritic tips in the OPL. TRPM1 antibody was used to mark the ON-BC puncta,

and PNA was used as a marker for cone synapses (yellow arrows). (**c**) Rod dendritic tip localization was confirmed with an alternative antibody (LRRTM4 B).

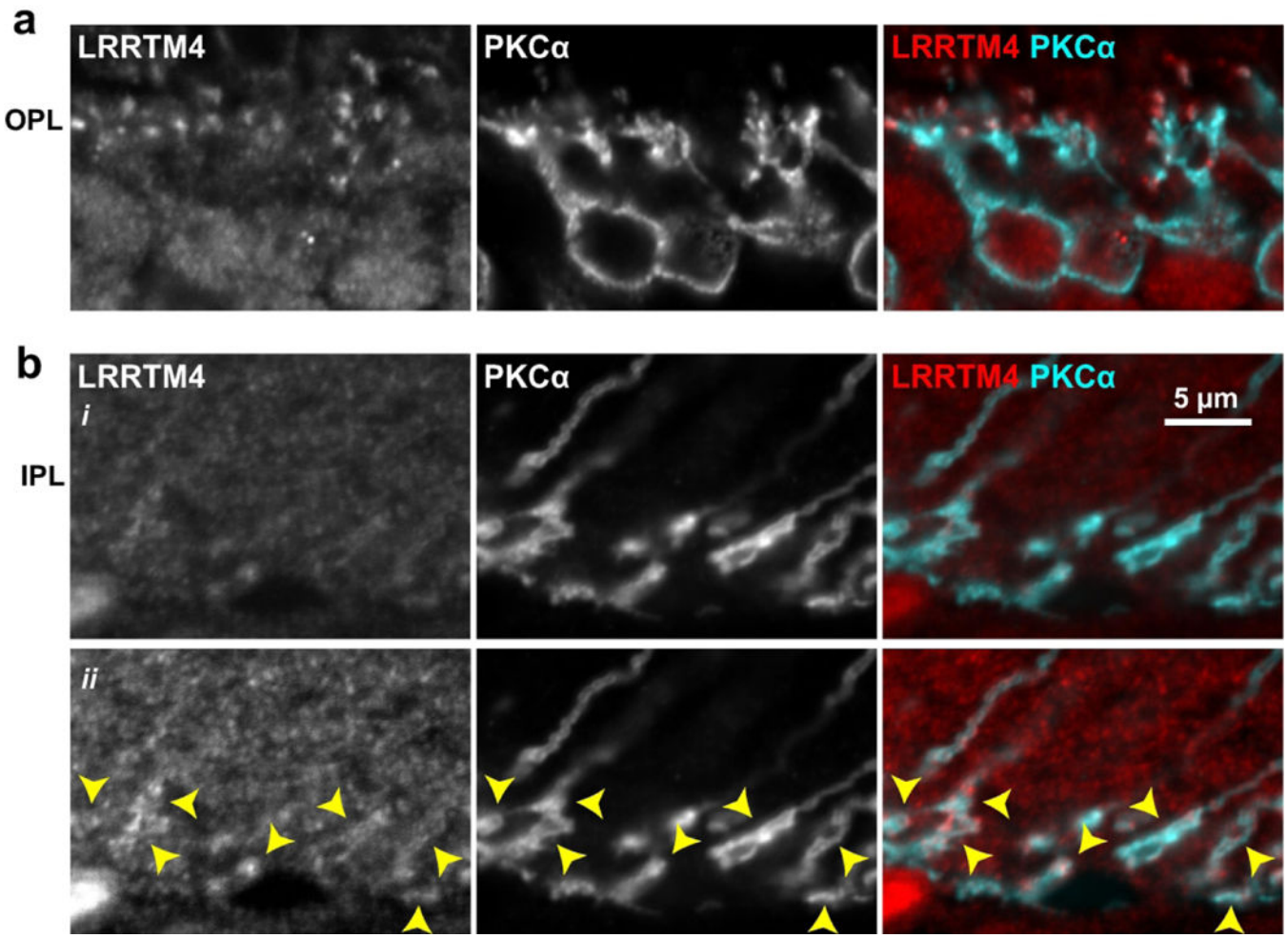

Figure 2. LRRTM4 immunostaining in the IPL.

Images showing the OPL (**a**) and IPL (**b**) of a retina section co-stained with LRRTM4 and rod BC marker PKCα. *i*, images were processed as in (a); *ii*, LRRTM4 channel levels were adjusted to show faint immunolabeling of rod BC terminals (arrowheads).

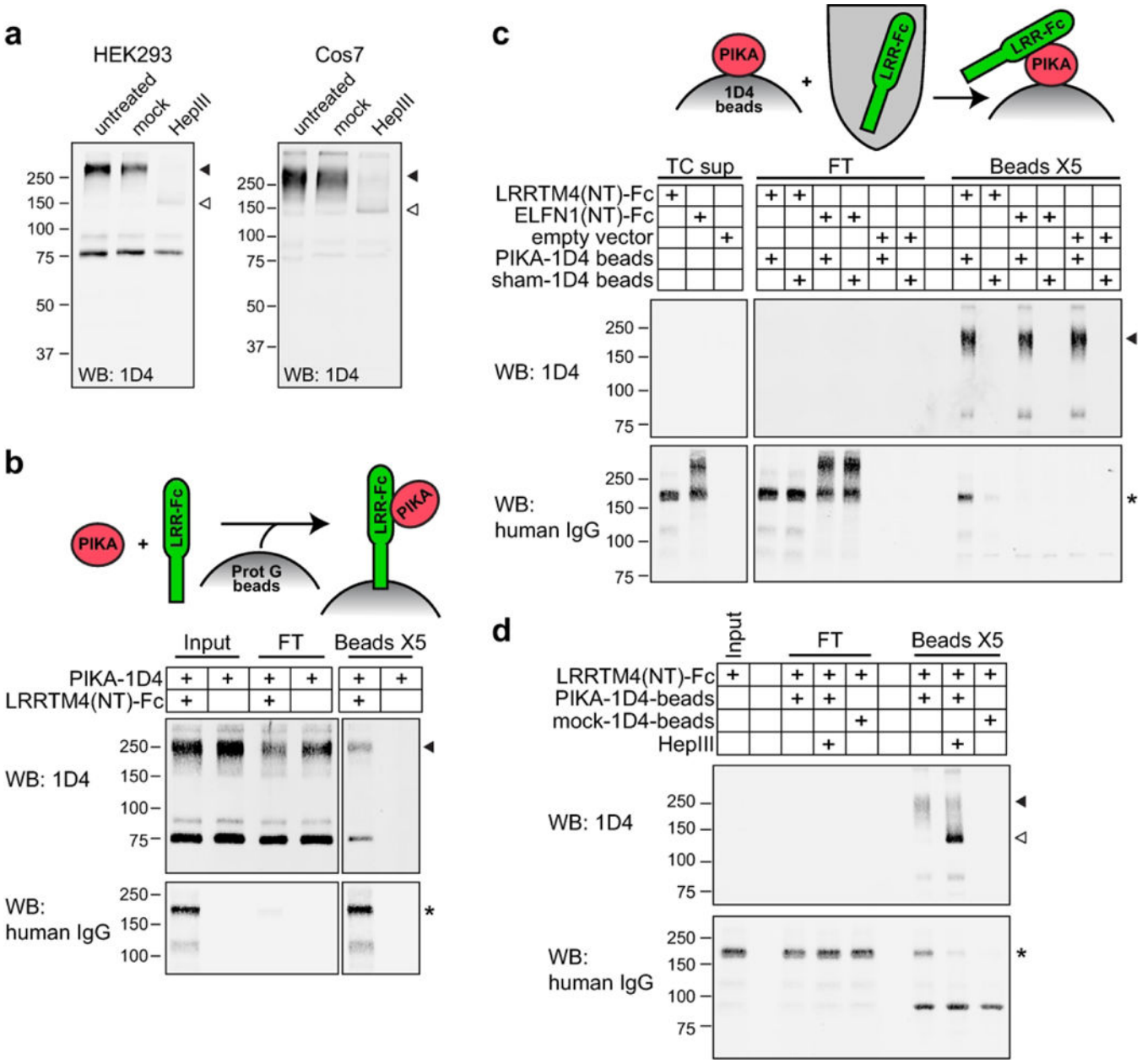

Figure 3. LRRTM4 extracellular domain interacts with pikachurin.

(**a**) Purification of pikachurin-1D4 from HEK293 or Cos7 cells resulted in a slow-migrating band (closed arrowhead), which was reduced to a fast-moving band (open arrowhead) upon treatment with heparinase (HepIII). (**b**) Purified pikachurin-1D4 (from HEK293 cells) was mixed with purified LRRTM4 extracellular domain fused to Fc (LRRTM4(NT)-Fc) (from HEK293 cells), and co-precipitated with protein G beads. (**c**) Bead-bound pikachurin-1D4 from Cos7 cell culture supernatant or control beads were mixed with cell culture supernatant (TC sup) from Cos7 cell cultures transfected with plasmids expressing LRRTM4(NT)-Fc, ELFN1(NT)-Fc, or empty vector. LRRTM4(NT)-Fc was specifically co-precipitated (asterisk). Similar results were observed with proteins expressed in HEK293 cells. (**d**) Bead-bound pikachurin-1D4 or control beads were treated with HepIII or mock-treated, then used

in the TC sup pull-down experiment as in (c). HepIIItreatment resulted in a faster-migrating pikachurin band (open arrowhead), and severe reduction in LRRTM4(NT)-Fc binding (asterisk).

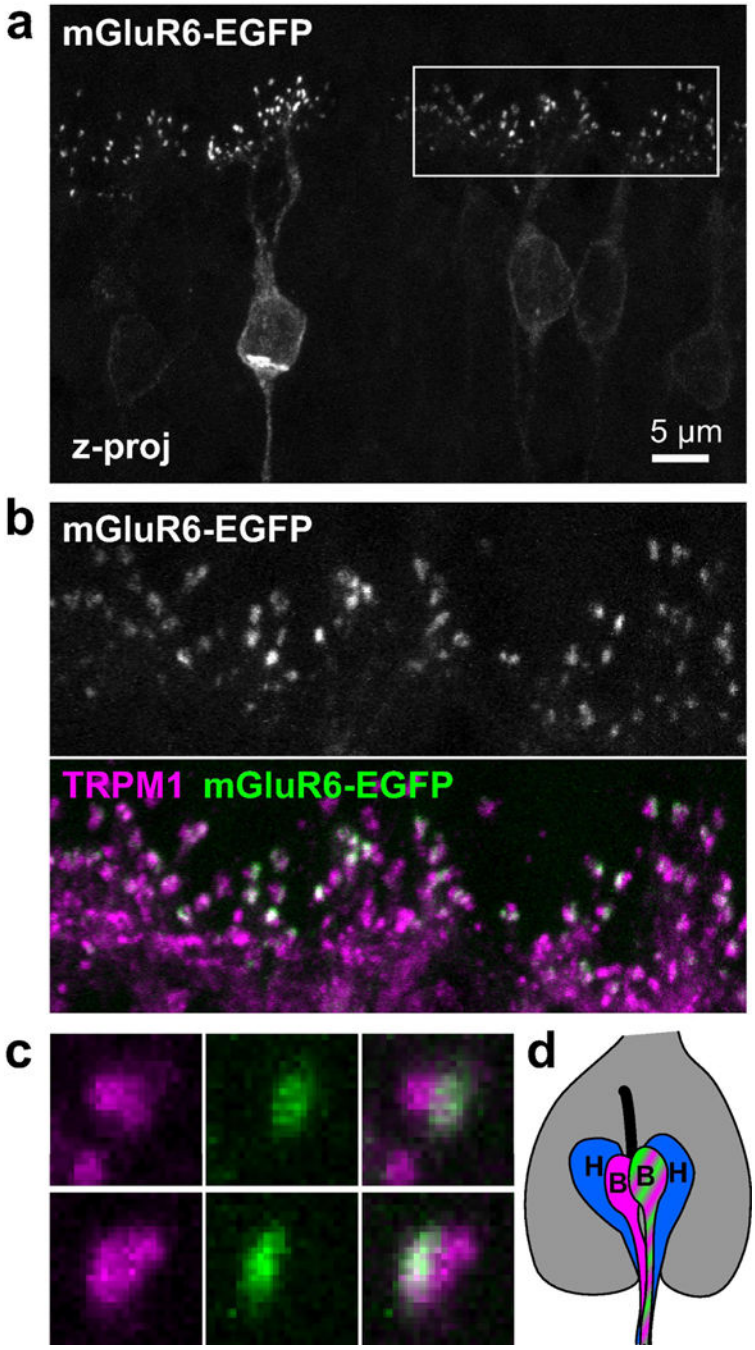

Figure 4. Electroporated mGluR6-EGFP is correctly localized to ON-BC dendritic tips.

(**a**) Z-projection from a confocal stack showing punctate expression of electroporated mGluR6-EGFP in the OPL. (**b**) Zoomed-in view of the boxed region in (a) showing colocalization with TRPM1 puncta, although many EGFP puncta appear smaller than the TRPM1 puncta. (**c**) Examples of puncta in which only one of the two BC dendritic tips is from an EGFP-expressing cell. (**d**) Cartoon depiction of a rod spherule with triad synapse composed of two horizontal cell processes (H) and two BC dendrites (B), one of which expresses EGFP.

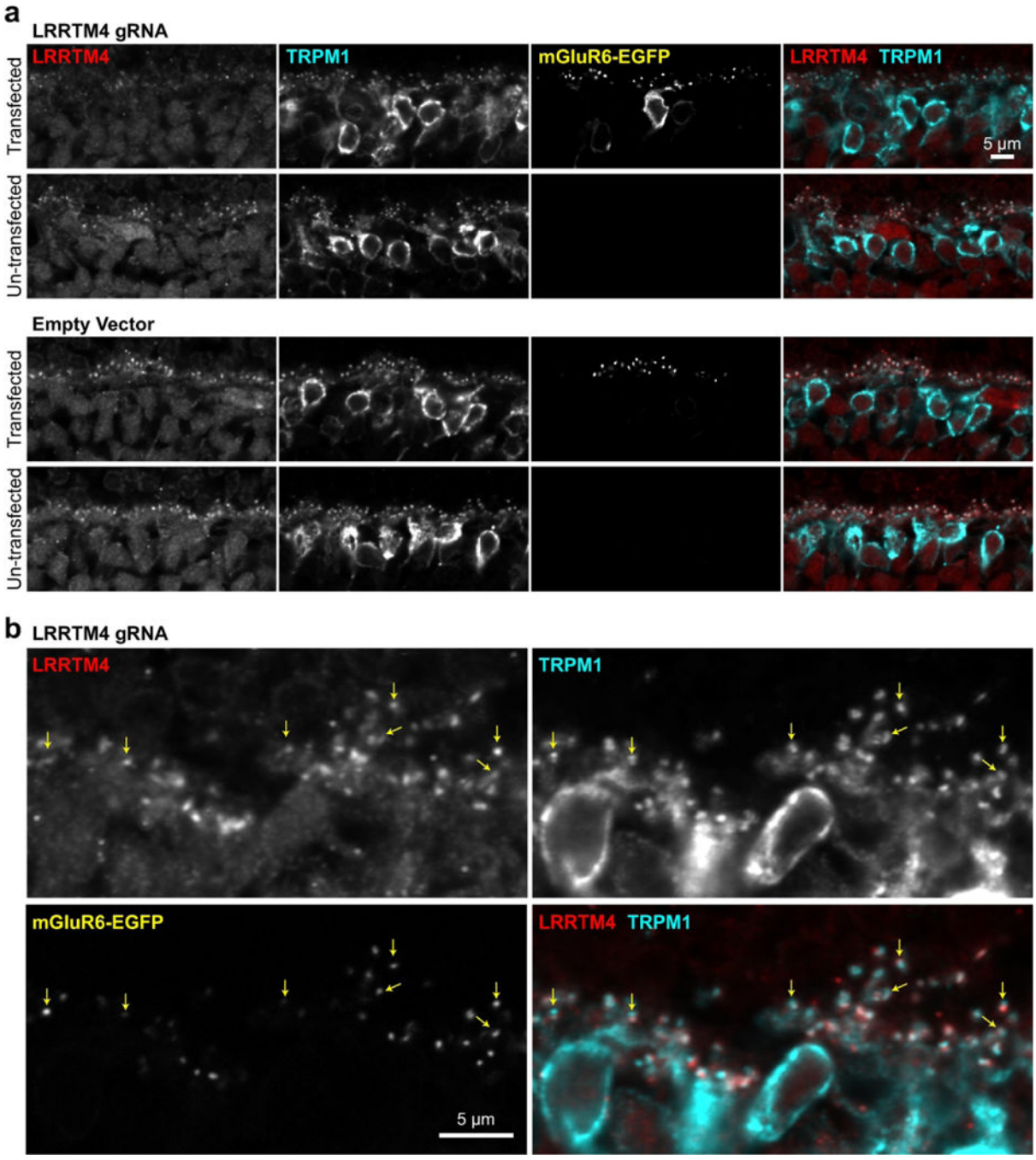

Figure 5. Co-electroporation of CRISPR/Cas9 and marker protein mGluR6-EGFP.

Retinas were electroporated with a plasmid expressing Grm6-promoter driven mGluR6-EGFP and either a mixture of two CRISPR plasmids expressing Grm6-promoter driven Cas9 with two different LRRTM4-targeting gRNAs, or a CRISPR plasmid with no gRNA (empty vector). (**a**) In some cases, LRRTM4 immunostaining was clearly reduced in gRNA-transfected regions, compared to untransfected regions from the same retina. However, in most cases, abnormalities in LRRTM4 immunostaining were not obvious at low magnification; example shown in (**b**). Yellow arrows indicate examples of puncta used in

subsequent analyses, where both BC dendritic tips can be detected, with one containing mGluR6-EGFP.

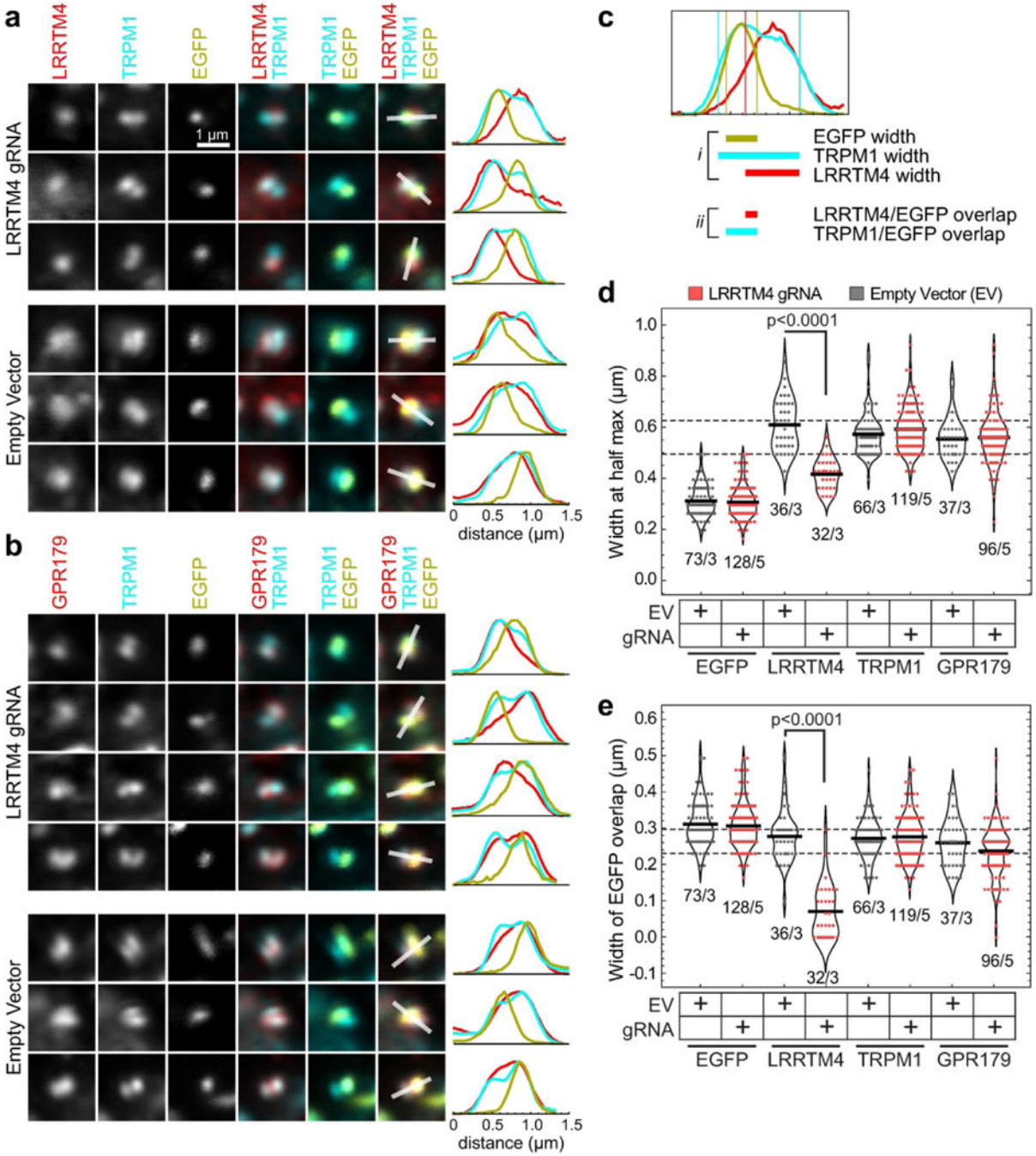

Figure 6. LRRTM4 expression is abolished in dendritic tips of transfected BCs.

(**a**) Gallery of example puncta from retinas electroporated with mGluR6-EGFP and gRNA or empty vector (EV) CRISPR plasmids, and immunostained for LRRTM4 and TRPM1. Lines used for intensity profiles are shown as white bars. Intensity profiles are at right, shown normalized to minimum and maximum values. In gRNA-expressing puncta, the LRRTM4 profile is narrower and has less overlap with mGluR6-EGFP, compared to control puncta. (**b**) Gallery of example puncta from retinas electroporated as in (a) and immunostained for GPR179 and TRPM1. Line intensity profiles for gRNA-expressing

puncta reveal a range of GPR179 phenotypes, ranging from severe (top) to normal (bottom). (**c**) Diagram illustrating quantification of width at half max (*i*) and EGFP overlap (*ii*) from line profiles. (**d,e**) Quantification of width (d) and EGFP overlap (e). Individual measurements are shown superimposed on violin plots. Numbers below each distribution indicate number of puncta and number of animals included. Measurements for EGFP in (e) are the same as EGFP width measurements shown in (d), and are reproduced to aid comparison with the other labels. Dashed lines show the 1st and 3rd quartiles of combined negative control data (LRRTM4 EV, TRPM1 EV, and GPR179 EV). LRRTM4 gRNA measurements were significantly different from LRRTM4 EV measurements ($p<0.0001$, t-test with Welch's correction). All other measurements were not significantly different from the corresponding EV control ($p>0.05$).

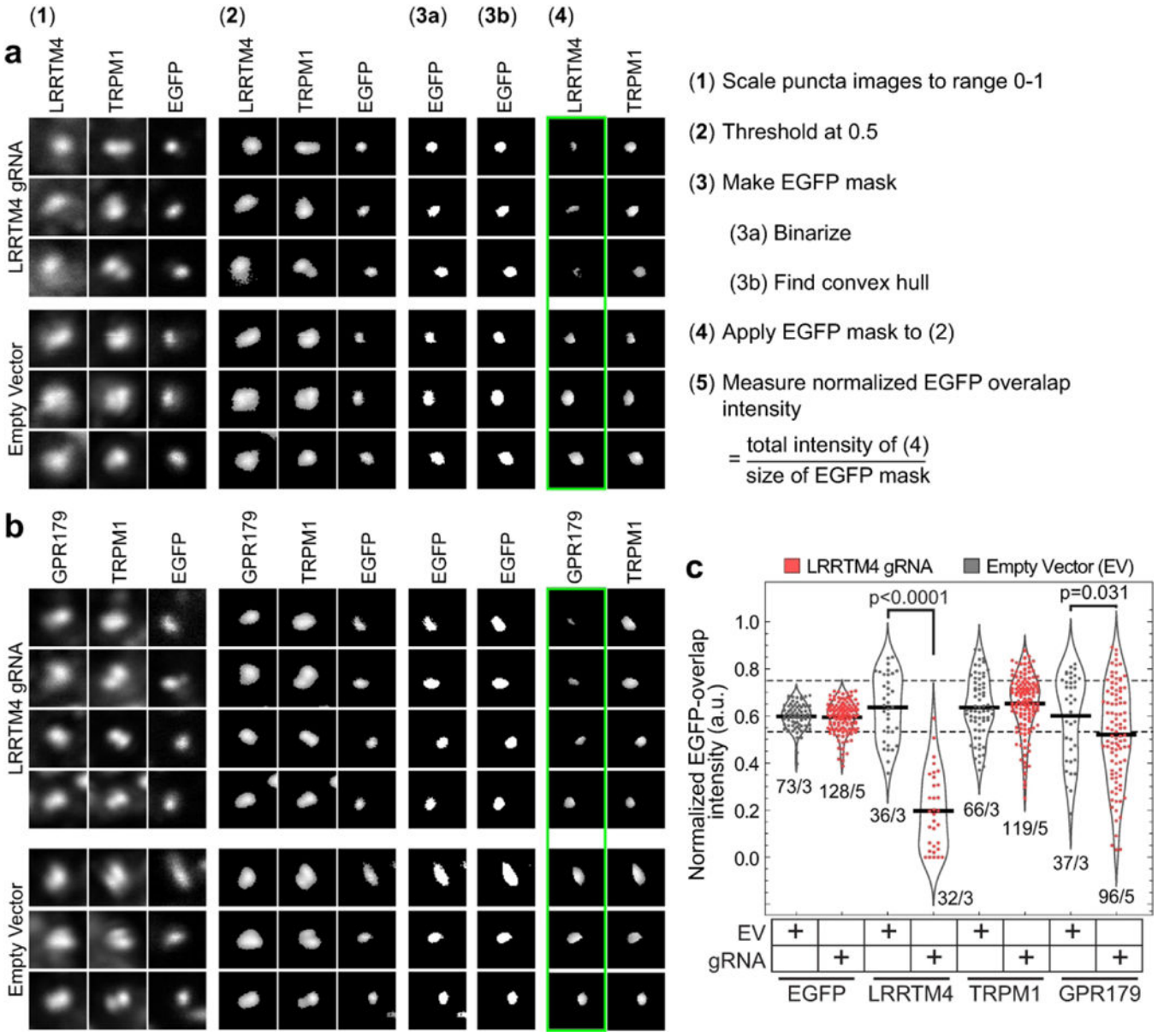

Figure 7. GPR179 expression is slightly reduced in dendritic tips of transfected BCs.

(**a,b**) Gallery of example puncta from retinas electroporated with mGluR6-EGFP and gRNA or EV CRISPR plasmids, and immunostained for TRPM1 and LRRTM4 (a) or GPR179 (b), shown at each stage of image processing. The reduced intensity of LRRTM4 immunostaining in the EGFP-overlap area is evident for gRNA-expressing puncta, compared to control puncta (step 4, green box). The intensity of GPR179 immunostaining in the EGFP-overlap area exhibited a range of phenotypes, from severe (top) to normal (bottom). (**c**) Quantification of normalized intensity in the EGFP-overlap area. Individual measurements are shown superimposed on violin plots. Numbers below each distribution indicate number of puncta and number of animals included. Dashed lines show the 1st and 3rd quartiles of combined negative control data (LRRTM4 EV, TRPM1 EV, and GPR179 EV). LRRTM4 and GPR179 gRNA measurements were significantly different from their

respective EV controls (p values as indicated, t-test with Welch's correction). All other measurements were not significantly different from the corresponding EV control ($p>0.05$).